Dynamical Processes of Block Evolution

BENJAMIN A. CASH AND SUKYOUNG LEE

Department of Meteorology, The Pennsylvania State University, University Park, Pennsylvania

(Manuscript received 19 February 1999, in final form 2 December 1999)

ABSTRACT

The dynamical processes associated with block evolution are investigated by analyzing a GCM run, forced with perpetual January conditions. The core of the analysis lies on the temporal evolution of the blocks and on vorticity budget terms obtained from appropriate compositing procedures on a 350-mb model output. The results from the budget analysis are examined with barotropic model experiments, which allow the investigation of the influence of an individual dynamical process on block evolution.

Results are presented for two composite blocks, one close to the Atlantic storm track and the other farther downstream. Although these two blocks are found to develop differently, they share the following characteristics. During the decay linear processes dominate, and the high- and low-frequency eddy fluxes contribute equally toward prolonging the lifetime of the blocks by 2 to 3 days. While the time average of the budget yields results that are consistent with previous diagnostic studies, it is shown that such an approach exaggerates the role played by high-frequency eddies.

The barotropic model experiments show that the nonlinear self-interaction of the composite block anomaly plays a minimal role in the block evolution. It is the remaining part of the composite low-frequency eddy flux that contributes significantly toward the block evolution, indicating that case-to-case variability of the individual blocking events can be substantial, and that the nonlinearity of a slowly moving, nonsteady component of the flow plays an important role for the individual blocking events. The model experiments also demonstrate that the effect of divergence is crucial for correctly reproducing the structure of the blocking high. The implications of these results, as they apply to some of the prominent blocking theories, are also discussed.

1. Introduction

One of the most striking features of atmospheric low-frequency variability is the phenomenon of blocking. Blocks are typically composed of a warm anticyclone at high latitudes, and are often accompanied by a lower-latitude cyclone. This structure may remain nearly stationary for periods upward of a week, during which time it deflects synoptic-scale eddies from their climatological paths. This persistent effect on the normal weather patterns makes understanding and predicting blocks critical to forecasting.

Most theoretical blocking studies focus on their maintenance mechanisms (e.g., McWilliams 1980; Shutts 1983), although initiation mechanisms have also been investigated (Fredrickson 1982; Colucci 1985; Mak 1991). One of the most widely studied and accepted maintenance mechanisms is forcing by high-frequency transient eddies (period less than 10 days), where the transient eddies are defined as having a smaller time-scale than that of the block. This mechanism originates with Berggren et al. (1949), who clearly depicted the accumulation of cutoff lows in lower latitudes and cutoff highs in higher latitudes at the upstream edge of the block. Known as eddy straining, this process was examined theoretically by Shutts (1983) and gained support from subsequent diagnostic studies (e.g., Illari 1984; Mullen 1987).

An equally viable maintenance mechanism focuses on the role played by the block itself. It is plausible that the ''high over low'' structure of some blocking events can be stationary with respect to the earth when the westward vorticity tendency induced by nonlinear self-interactions cancels the eastward tendency due to linear dispersion of the block. This conjecture received support from studies such as Branstator and Opsteegh (1989) and Anderson (1992), which found nearly stationary states that resemble observed blocking patterns.

The above theories focus primarily on blocking maintenance mechanisms. Similarly, most diagnostic studies of blocking events describe time-averaged characteristics (e.g., Illari 1984; Mullen 1986, 1987). These studies conclude that nonlinear vorticity flux convergence by transient eddies maintains the blocks against linear dispersion, consistent with the above two theories. However, Feldstein (1998) points out a possible pitfall when

Corresponding author address: Dr. Sukyoung Lee, Dept. of Meteorology, The Pennsylvania State University, 503 Walker Bldg., University Park, PA 16802.
E-mail: sl@essc.psu.edu

examining the time average of a low-frequency anomaly if the averaging period equals or exceeds the lifetime of the anomaly. Consider the linearized vorticity equation for a low-frequency anomaly,

$$\frac{\partial \psi'}{\partial t} = L\psi' + N, \tag{1}$$

where the prime denotes an unspecified low-frequency, for example, greater than 10 days, deviation from the time mean; L is the linear operator; and N the low-frequency contribution from nonlinear interactions. The quantity N includes nonlinear interactions between low-frequency transients, high-frequency transients, as well as low–high cross-frequency interactions. Because the time average of the left-hand side (lhs) of (1) must be small, averaging over a period longer than the lifetime of the anomaly must show an approximate balance between $\overline{N}$ and $\overline{L\psi'}$, where the overbar denotes time mean. If $L\psi'$ changes sign during the block evolution, then the magnitude of $\overline{L\psi'}$ can be much smaller than most instantaneous values of $L\psi'$. In this case, the above balance requires that the magnitude of $\overline{N}$ must also be much smaller than $L\psi'$ at most times. Therefore, although a nonzero $\overline{N}$ may imply the presence of a nonlinear feedback, it is possible that this feedback is of only secondary importance.

In light of the drawback outlined above, we feel that the full temporal evolution of blocking events must be examined to gain an unbiased view of the blocking process. For this purpose, we focus on the the composite temporal evolution of each term in the vorticity equation during blocking events. This analysis not only allows us to evaluate the relative roles of the high-frequency transient eddies, that is, the eddy straining mechanism, and the low-frequency self-interaction of the blocking flow, but also other processes that have not been widely considered. While there are studies that examine the temporal evolution of blocking events (e.g., Nakamura and Wallace 1993; Nakamura et al. 1997), they do not examine the complete vorticity budget. Rather, they focus on the role of the high-frequency transient eddies.

We complement the above investigation with a hierarchy of barotropic model calculations. An inherent disadvantage of any budget analysis is, in general, that the processes represented by each term in the budget are *not* linearly independent. Thus, each term's evolution may be influenced by the other terms, preventing one from making firm conclusions about the role of each term. The barotropic model experiments address this disadvantage.

The paper is organized as follows. Section 2 describes the data and analysis methods used. The results of the vorticity budget are presented in section 3, while section 4 describes the barotropic model experiments and their results. A general discussion of the results follows in section 5.

2. Data and methodology

a. Dataset

This study uses data generated by a 2100-day run of a Geophysical Fluid Dynamics Laboratory (GFDL) perpetual January general circulation model (GCM). This GCM has nine vertical sigma levels, rhomboidal 30 truncation, realistic topography, and climatological January SSTs. The parameterizations for physical processes such as cloud formation are described in Gordon and Stern (1982). For purpose of comparison with other studies, our results have been logarithmically interpolated to pressure surfaces. Studies by Blackmon et al. (1986) among others have shown the climatology and structure of blocking events in GCMs to be similar to observations. Thus, we make use of the internal consistency of GCM data to determine the vorticity budget far more accurately than possible with observational data (Cai and van den Dool 1994; Feldstein 1998), with reasonable confidence that our results are representative of real blocks.

b. Blocking criteria

We use a modified version of the Kaas and Branstator (1993) criteria for identifying blocks. We first digitally low-pass filter (>10 days, and excluding the time mean; all low-pass filtered quantities will be denoted by a superscript L) the 350-mb meridional winds for all grid points in the Northern Hemisphere. These grid points are then examined to determine whether they satisfy the criteria for being a blocking candidate. Grid points are considered to be blocking candidates if $v^L > 10$ m s^{-1} within 1000 km upstream and $v^L < -10$ m s^{-1} within 1000 km downstream, ensuring that the point lies within a region of anticyclonic circulation. For points failing to meet this criteria, we check the immediately adjacent points. If any of these points satisfy the criteria, the original point is also considered to be a candidate.

Once the set of candidates is defined, any point that remains a candidate for 10 or more consecutive days is considered to be part of a blocking event. To ensure separation of events for compositing and filtering purposes, two events occurring less than 10 days apart are treated as a single event. Block duration is then defined as the total number of days that a point satisfies the candidacy criteria, in addition to any period between combined events. Block onset is defined as the first day a point satisfies the blocking candidacy criteria. We use data at the 350-mb level because we find blocks attain their maximum amplitude near this level. For this study, we consider only those events occurring poleward of 20°N and from 90°W to 90°E.

While many studies (e.g., Dole and Gordon 1983; Mullen 1986, 1987) define blocking through geopotential height anomalies, these definitions suffer certain drawbacks (Kaas and Branstator 1993; Liu 1994) to which the meridional wind definition is less susceptible.

Height anomaly criteria may identify teleconnection patterns, strong ridges, or standing wave fluctuations as blocking events, when an examination of the full field shows nothing a synoptician would label a block.

c. Vorticity budget

The primary analysis performed in this study is the calculation of detailed vorticity budgets for composite blocking events. Following Cai and van den Dool (1994) and Feldstein (1998), we decompose the low-pass filtered streamfunction tendency equation (∇^{-2} of the vorticity equation), allowing us to determine quantitatively the contribution of different terms in the equation to block evolution.

The streamfunction tendency equation can be written as

$$\frac{\partial \psi^L}{\partial t} = \sum_{i=1}^{8} \xi_i + R, \tag{2}$$

where the ξ_i are

$$\xi_1 = \nabla^{-2}\left[-(v_r^L + v_d^L)\frac{1}{a}\frac{df}{d\theta}\right]$$

$$\xi_2 = \nabla^{-2}(-[\overline{\mathbf{v}}_r]\cdot\nabla\zeta'^L - \mathbf{v}_r'^L\cdot\nabla[\overline{\zeta}]) + \nabla^{-2}(-[\overline{\mathbf{v}}_d]\cdot\nabla\zeta'^L - \mathbf{v}_d'^L\cdot\nabla[\overline{\zeta}])$$

$$\xi_3 = \nabla^{-2}(-\overline{\mathbf{v}_r^*}\cdot\nabla\zeta'^L - \mathbf{v}_r'^L\cdot\nabla\overline{\zeta^*}) + \nabla^{-2}(-\overline{\mathbf{v}_d^*}\cdot\nabla\zeta'^L - \mathbf{v}_d'^L\cdot\nabla\overline{\zeta^*})$$

$$\xi_4 = \nabla^{-2}[-(f + \overline{\zeta})\nabla\cdot\mathbf{v}_d'^L - \zeta'^L\nabla\cdot\overline{\mathbf{v}}_d]$$

$$\xi_5 = \nabla^{-2}(-\mathbf{v}_r'^L\cdot\nabla\zeta'^L)^L + \nabla^{-2}[-\nabla(\mathbf{v}_d'^L\zeta'^L)]^L$$

$$\xi_6 = \nabla^{-2}(-\mathbf{v}_r'^H\cdot\nabla\zeta'^H)^L + \nabla^{-2}[-\nabla(\mathbf{v}_d'^H\zeta'^H)]^L$$

$$\xi_7 = \nabla^{-2}(-\mathbf{v}_r'^L\cdot\nabla\zeta'^H)^L + \nabla^{-2}[-\nabla(\mathbf{v}_d'^L\zeta'^H)]^L + \nabla^{-2}(-\mathbf{v}_r'^H\cdot\nabla\zeta'^L)^L + \nabla^{-2}[-\nabla(\mathbf{v}_d'^H\zeta'^L]^L$$

$$\xi_8 = \nabla^{-2}[-\boldsymbol{k}\cdot\nabla\times(\omega'^L\delta\overline{\mathbf{v}}/\delta p)] + \nabla^{-2}[-\boldsymbol{k}\cdot\nabla\times(\overline{\omega}\delta\mathbf{v}'^L/\delta p)] + \nabla^{-2}[-\boldsymbol{k}\cdot\nabla\times(\omega'\delta\mathbf{v}'/\delta p)]^L,$$

and ψ is the streamfunction, ζ the relative vorticity, $\mathbf{v}$ the horizontal wind vector, v the meridional wind component, ω the vertical wind component, a the earth's radius, and f the Coriolis parameter. The superscript H refers to high-pass filtered quantities. The subscripts d and r denote the divergent and rotational components of the horizontal wind, respectively. An overbar denotes the time mean, and primed values a deviation from the time mean. Square brackets are zonal averages, and asterisks the zonal deviations.

The physical interpretations of the ξ_i terms are as follows. The advection of the planetary vorticity by the low-frequency meridional winds is ξ_1. The interaction between the climatological zonal mean flow and the low-frequency transients is ξ_2, while ξ_3 is the interaction between the low-frequency transients and the climatological zonally asymmetric flow. The low-frequency contribution to the divergence is represented by ξ_4. Terms ξ_5 and ξ_6 represent the low- and high-frequency nonlinear interactions, respectively, while ξ_7 is due to the interaction between the high- and low-frequency transients. Term ξ_8 is the sum of the vertical vorticity advection and the stretching and tilting terms. Finally, R is a measure of the inaccuracies in the budget. These inaccuracies arise through interpolation from sigma to pressure levels, as well as through sampling problems introduced by saving the model output at one time step each day, rather than at every time step. Because ξ_7 and ξ_8 are very small, we also incorporate their effects into R. We will find R to be significantly smaller than the terms of interest in (2).

d. Vorticity pattern covariance

The covariance between a set of fields A_i and a field B is defined as

$$P_i = \sum_j A_{ij}B_j\cos(\theta_j), \tag{3}$$

where P_i is the covariance between A_i and B; A_{ij} and B_j are the values of A_i and B, respectively, at grid point j; and the product is weighted by the cosine of the latitude θ_j. In this study, all covariances are performed over the region poleward of 20°N and from 90°W to 90°E.

3. Results

a. Climatology and synopsis of blocking events

Figure 1 shows the distribution of blocking events identified by our criteria for the 2100 days of the dataset. A region of maximum blocking frequency lies over the northeastern Atlantic and western Europe, in good agreement with previous model studies (Blackmon et al. 1986; Kaas and Branstator 1993) and observations (Kaas and Branstator 1993). To explore possible variations in blocking mechanisms with respect to the location of the climatological stormtrack, we examine composites of the events at two grid points, denoted by ''A'' and ''B'' in Fig. 1. Point A (23 events) lies near the center of the 350-mb storm track, and point B (27 events) lies farther downstream. Point B is the point at which we find the maximum number of events. Throughout this paper, we refer to these points as the upstream and downstream cases, respectively. That we should expect to find systematic differences in the blocking mechanisms at these two points is suggested by Nakamura et al. (1998), who found that the relative importance of the high-frequency eddy vorticity flux divergence varies with location.

Figure 2 shows the composite evolution of the 350-mb low-pass streamfunction anomaly for the down-

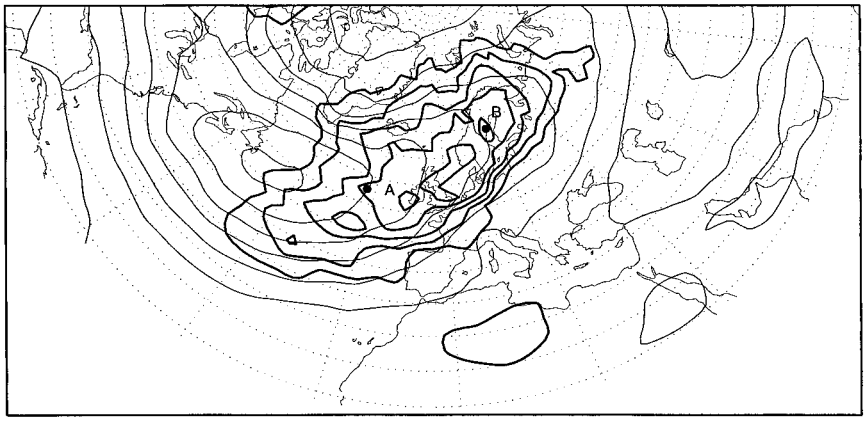

FIG. 1. The number of blocking events and the storm track structure at 350 mb. Heavy contours are number of identified blocks, and the contour interval is 5. Light contours are time-mean high-pass eddy kinetic energy, with a contour interval of 10 $m^2\ s^{-2}$. The zero contour is omitted.

stream case at lag −5, lag 0, lag +5, and lag +10 days. Block formation and evolution are clearly captured in this sequence, with the dominant anticyclone moving northeastward from southwest of the British Isles and becoming nearly stationary over Scandinavia. The block experiences weak growth prior to onset (Figs. 2a,b), then increases to its maximum amplitude at lag +5 (Fig. 2c) while continuing to drift slowly to the northeast.

The evolution of the upstream case shows wave train characteristics, in contrast to that of the downstream case, which mostly shows in situ development. A wave train exists over the Pacific Ocean at lag −5 (Fig. 3a). All anomalies other than the negative center over the western United States exceed the 95% confidence level, indicating that this pattern is not simply an artifact of the analysis. By onset (Fig. 3b), the wave train has intensified and new centers develop over North America and the North Atlantic Ocean. From Figs. 3a–d, it is apparent that the wave group propagates downstream more rapidly than the individual waves, suggesting that the blocking anomaly forming in the mid-Atlantic is associated with downstream energy flux. As the block reaches its maximum amplitude at lag +5 (Fig. 3c), we see the development of a cyclone to the south of the mature block, the canonical high over low pattern. The three main centers of the wave train remain quasi-stationary through lag +10 (Fig. 3d).

b. Pattern covariance and budget

We use the pattern covariance technique described in section 2d to quantify the contribution of different terms on the right-hand side (rhs) of (2) to the growth and decay of the blocking pattern. Thus, in (3), we identify various combinations of terms on the rhs of (2) with A_{ij}, and the maximum amplitude blocking pattern, rather than the instantaneous anomaly pattern, with B_j. Before examining the pattern covariances of various budget terms, we need to ensure that the budget is reasonably well balanced. Figure 4 shows the error term R at the time of maximum block amplitude (i.e., lag +5) for the downstream case. As can be inferred from Figs. 6 and 7, the error is substantially less than the individual budget terms in the blocking region.

Figures 5a and 5b show the covariance between the maximum anomaly pattern and the linear interaction term ($\Sigma_{i=1}^{4}\ \xi_i$), the low-frequency nonlinear term (ξ_5), and the high-frequency nonlinear term (ξ_6) for the downstream and upstream cases, respectively. The covariance between the total ($\Sigma_{i=1}^{6}\ \xi_i$) and the maximum anomaly is provided for reference. For both cases, during the onset (the period leading up to lag 0) and the decay (the period after the total covariance becomes negative) phases of the block, the linear term dominates. The sign change from a positive to a negative value occurs between lag +2 and lag +4 days for the linear term, and between lag +5 and lag +6 for the sum of the budget terms. Apparently, nonlinear terms must be responsible this difference in the timing of the sign change, indicating that the nonlinear terms prolong the life span of the block by 2 to 3 days. Indeed, the covariances of the nonlinear terms (Figs. 5a,b) show positive values throughout most of the maintenance (the period between the growth and decay phases) and decay phases of the block.

While the covariances for the two cases are broadly similar, important differences exist. For the downstream case the low-frequency nonlinear term is comparable to the linear term during the block formation and remains positive throughout the event, while in the upstream case it is much smaller than the linear term at most lags, consistent with the role of the wave train, as suggested by Fig. 3. This contrasts with the high-frequency nonlinear term, whose covariance is very similar for the two cases, and which plays an increasingly important role as the block approaches its maximum amplitude.

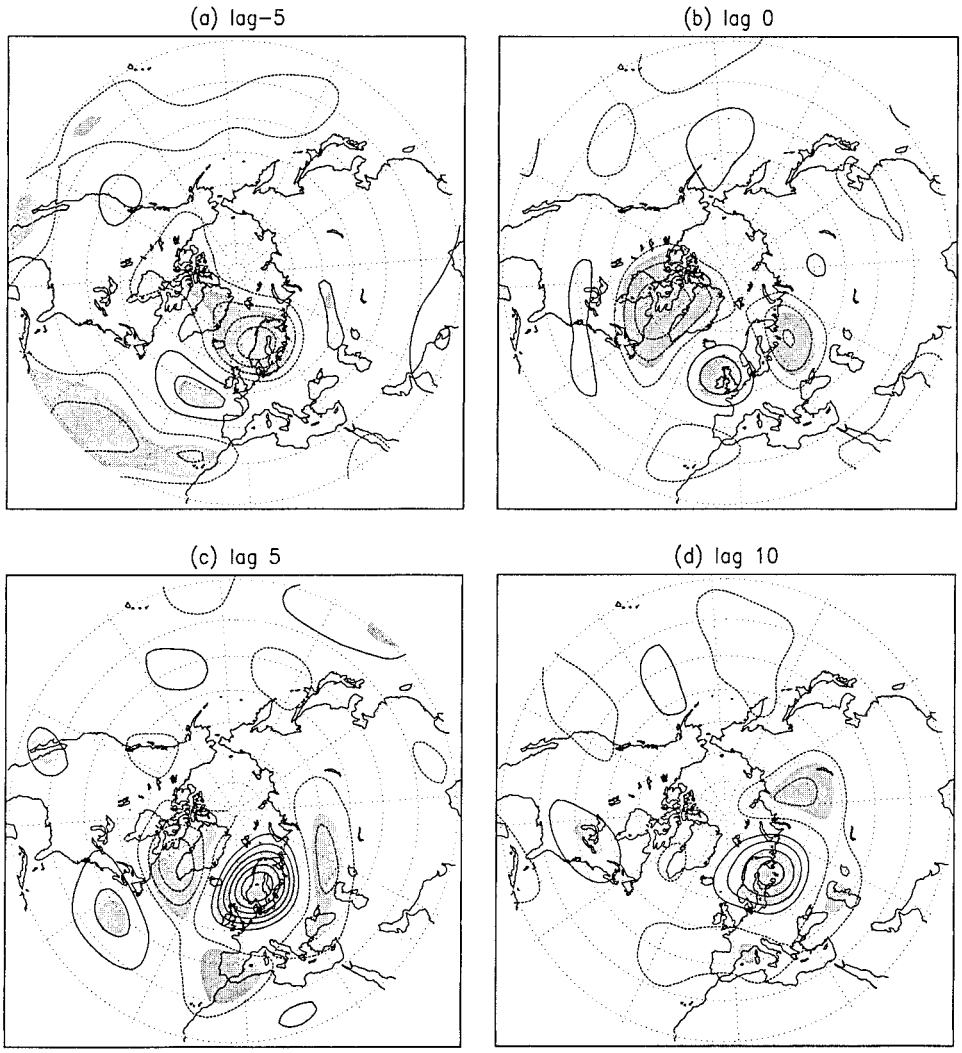

FIG. 2. Low-pass composite streamfunction anomaly for the downstream case at (a) lag −5, (b) lag 0, (c) lag +5, and (d) lag +10. Solid contours are positive, and dashed contours are negative. The contour interval is 2×10^6 m^2 s^{-1} with the zero contour omitted. Shading denotes the 95% confidence level from a two-tailed t test.

Although the above analysis provides a concise summary of the temporal evolution of the blocks, because there is no reason not to expect that important contributions to the covariances could come from peripheral features of the blocking, it is important to examine the budget in greater detail. Figures 6 and 7 show contours of the sum of the linear interaction terms ($\Sigma_{i=1}^{4}\,\xi_i$), the low-frequency nonlinear term (ξ_5), the high-frequency nonlinear term (ξ_6), and their total ($\Sigma_{i=1}^{6}\,\xi_i$), at onset and at lag +10 days, respectively, for the downstream case. Superimposed on these contours is shading that illustrates the anomalous streamfunction field at lag +5 days, the time of the blocking maximum.

Figures 6b and 7b clearly show that it is the blocking high, not the other lesser important features, that dominates the contribution to both the positive and negative covariances of the linear terms at onset and lag +10 days, respectively. The same is true for the high- and low-frequency nonlinear terms. Also, consistent with the time evolution of the covariances as described above, the low-frequency nonlinear term undergoes a substantial structural change over the blocking high (cf. Figs. 6c and 7c). In comparison, changes in structure of the high-frequency nonlinear term are relatively small (cf. Figs. 6d and 7d), contributing a positive projection onto the blocking high at both the onset and at lag +10. Thus, although the projection of the high-frequency nonlinear term onto the blocking high does not dominate at any given time, it is more persistent than any other terms in producing positive tendencies over the blocking region.

Although not shown for brevity, as can be inferred

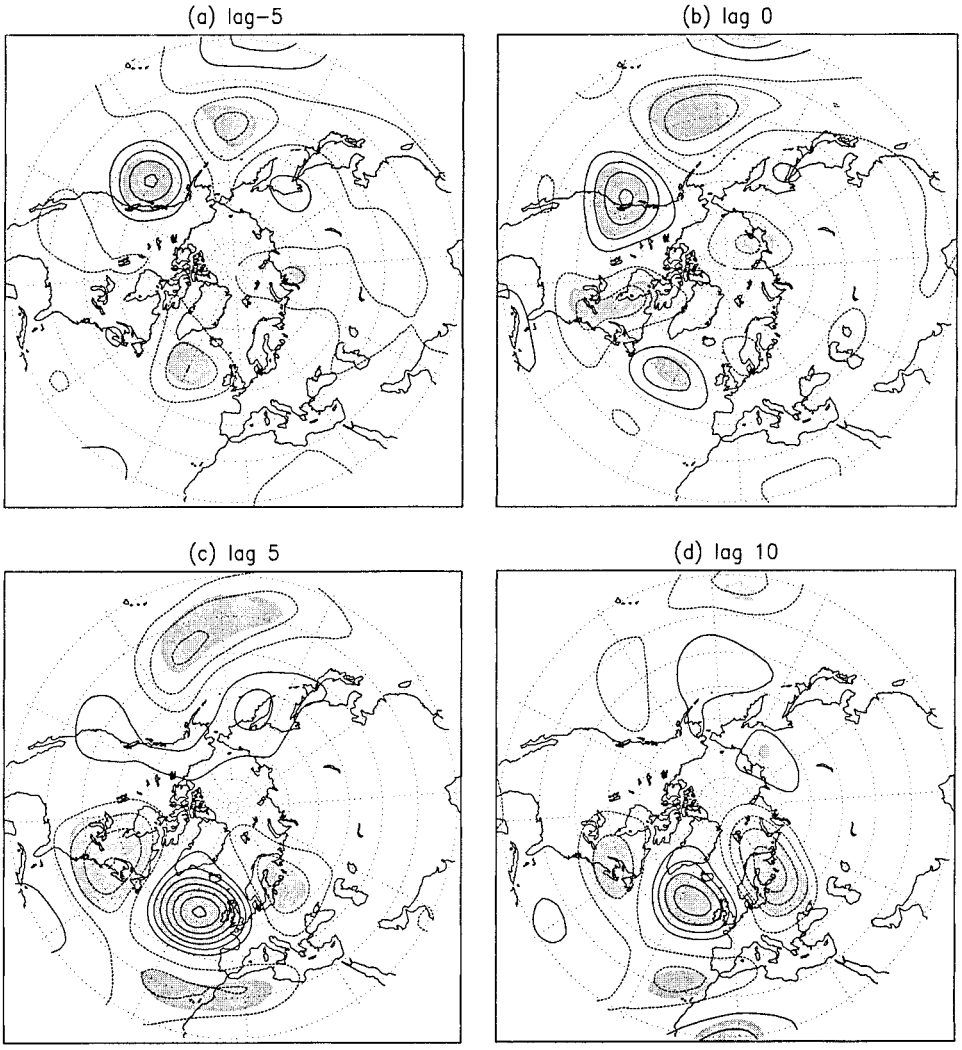

FIG. 3. As in Fig. 2 but for the upstream case.

from Figs. 5a and 5b, the characteristics of various budget terms for the upstream case are very similar to those for the downstream case, except as stated above that the low-frequency nonlinear term plays a lesser role for the onset of the block.

4. Barotropic model

As noted in the introduction, an inherent drawback in any budget analysis is the assumption that individual terms may be analyzed independently. In reality, each term in the streamfunction tendency equation modifies the blocking anomaly and the surrounding flow, and thus affects the evolution of every other term. To address this ambiguity, we perform a series of numerical experiments using a barotropic model, designed to investigate quantitatively the importance of individual terms over the lifetime of the event. These experiments are an extension of a similar study by Nakamura et al. (1997), who considered the high-frequency nonlinear interactions as the only external forcing.

We integrate

$$\frac{\partial \nabla^2 \psi'}{\partial t} + [J(\psi', \nabla^2 \overline{\psi} + f) + J(\overline{\psi}, \nabla^2 \psi') + J(\psi', \nabla^2 \psi')] = -\kappa \nabla^{10} \psi' + F_o, \quad (4)$$

where ψ' is the streamfunction anomaly, $\overline{\psi}$ the time-mean streamfunction, f the Coriolis parameter, ∇^2 the horizontal Laplacian in spherical coordinates, J the Jacobian, and F_o is a ''forcing'' term denoting those processes not represented in a nondivergent barotropic model. The forcing term F_o includes the effect of 1) the high-frequency transients, 2) the divergence term, and 3) an important component of the low-frequency nonlinear term.

For proper interpretation of the results, the latter two forcing terms warrant additional remarks. Although we

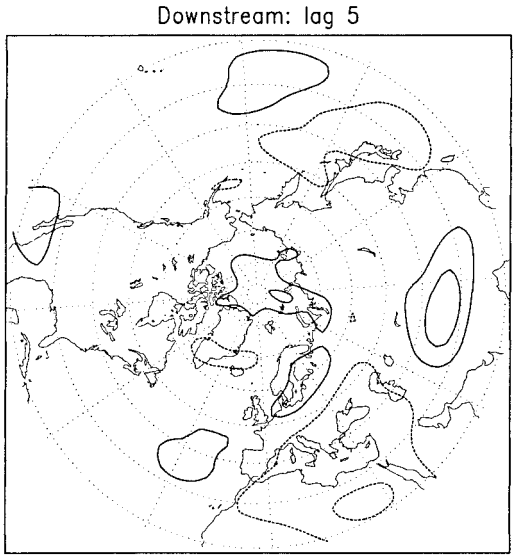

FIG. 4. Composite error R at lag +5 for the downstream case. Solid (dashed) contours are positive (negative) and the zero contour is omitted. The contour interval is 5 m^2 s^{-2}.

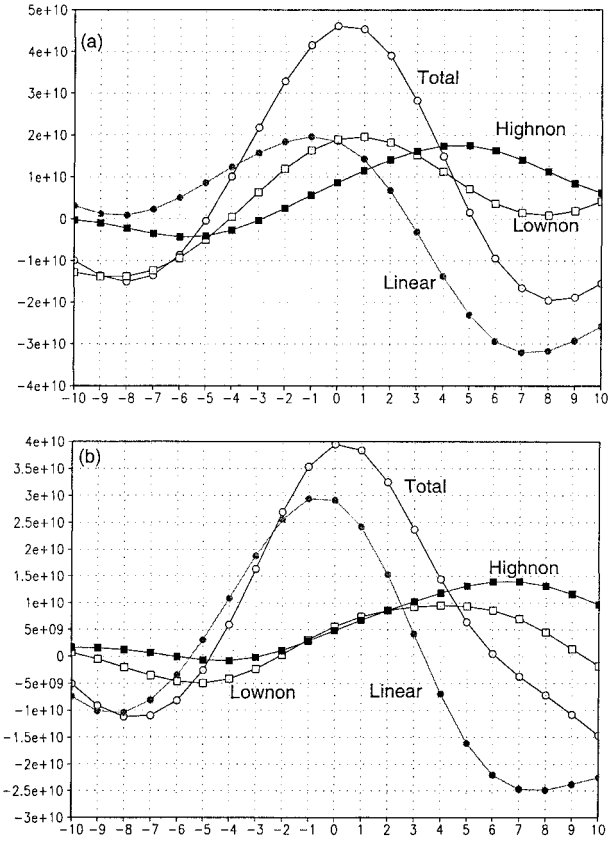

FIG. 5. Covariance between the budget terms and the lag +5 streamfunction anomaly for (a) the downstream case and (b) the upstream case. "Total" = $\Sigma_{i=1}^{6}\,\xi_i$, "Linear" = $\Sigma_{i=1}^{4}\,\xi_i$, "Lownon" = ξ_5, and "Highnon" = ξ_6.

write the divergence term as a separate forcing, given that the vorticity fluxes,[1] including both the linear and nonlinear terms, induce secondary circulations (e.g., omega equation), it is misleading to treat the divergence term as an entity separate from the other terms. Therefore, we anticipate that the divergence term is driven in part by the vorticity fluxes and also by Ekman pumping. Evidently, the part of the divergence not accounted for by the Ekman pumping can either prolong or shorten the blocks' lifetime. This perspective should be kept in mind when intepreting the results.

Next, in order to interpret the third forcing term above, we expand the low-frequency nonlinear transient term as follows:

$$\nabla \cdot (\boldsymbol{v}^L\zeta^L) = \nabla \cdot (\boldsymbol{v}_c^L\zeta_c^L) + \nabla \cdot (\boldsymbol{v}_*^L\zeta_c^L) + \nabla \cdot (\boldsymbol{v}_c^L\zeta_*^L) + \nabla \cdot (\boldsymbol{v}_*^L\zeta_*^L), \quad (5)$$

where c denotes the composite value, and "*" the deviation from the composite value. The first term on the rhs of (5), referred to as the "self-induced" nonlinear term, corresponds to the fourth term on the lhs of (4). Note that the same quantity is often called stationary nonlinearity (e.g., Branstator 1992). We treat the latter three terms on the rhs of (5) as a part of the "external forcing," F_o, and refer to the sum of these terms as the "incoherent nonlinear term," as it represents the component of the low-frequency nonlinear term not captured by the composite anomaly.

However, it is somewhat misleading to interpret all of the incoherent nonlinear term as external forcing for the block. This is because the incoherent nonlinear term represents the case-to-case varibility of the low-frequency flow associated with the individual blocking events. Therefore, for individual blocking events, it is the sum of the incoherent nonlinear term and the self-induced nonlinear term that accounts for the actual self-induced nonlinearity. Despite this ambiguity, we separate the incoherent nonlinear term in order to highlight that most of the low-frequency nonlinear term can be accounted for by this term, which was neglected in similar calculations by Nakamura et al. (1997).

We initialize the model with the composite streamfunction anomaly 3 days prior to the lag of interest, and then integrate forward in time. We focus here on three lags: lags 0, +5, and +10, which represent onset, maximum, and decay, respectively. These runs are performed for both the upstream and the downstream cases. The forcing terms, F_o, are determined by a temporal linear interpolation of their composite values. The value of the scale-selective diffusion coefficient, κ, is 8×10^{37} m^8 s^{-1}. The model is run at R30 resolution, consistent with the GCM data.

[1] For the sake of simplifying the discussion to be followed, the effect of the heat flux on the secondary circulation is not mentioned here.

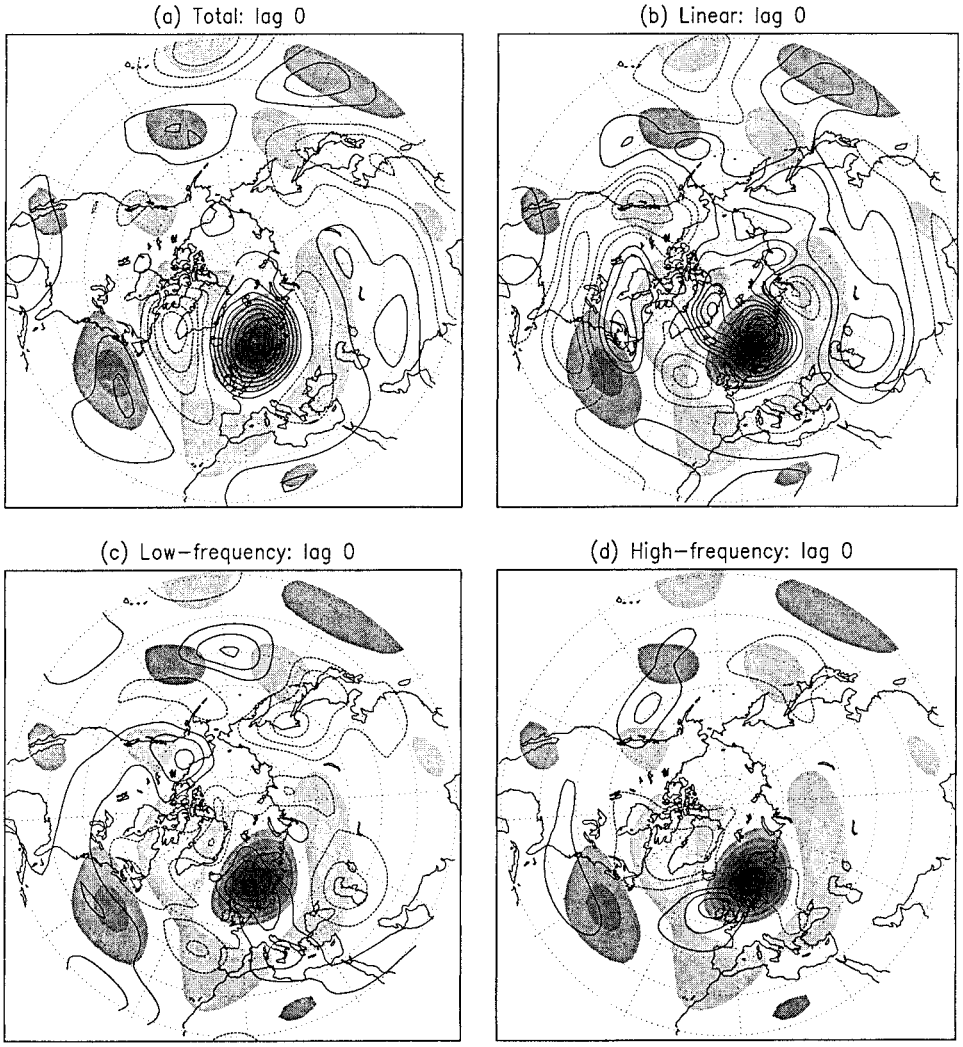

FIG. 6. Composite of (a) the sum of the budget terms, $\Sigma_{i=1}^{6}\,\xi_i$; (b) the linear term, $\Sigma_{i=1}^{4}\,\xi_i$; (c) the low-frequency nonlinear term, ξ_5; and (d) the high-frequency nonlinear term, ξ_6, at lag 0 for the downstream case. Solid contours are positive, dashed contours are negative, and the zero contour is omitted. The contour interval is 5 $m^2\,s^{-2}$. Dense (light) shading indicates positive (negative) values of the composite streamfunction anomaly at lag +5. Shaded areas denote absolute values exceeding $2 \times 10^6\ m^2\ s^{-1}$. The shading interval is $2 \times 10^6\ m^2\ s^{-1}$.

If the individual forcing terms in the budget are essentially independent, we expect

$$(\psi_T^f - \psi_0^f) \approx \sum_{N=1}^{3} (\psi_N^f - \psi_0^f), \tag{6}$$

where ψ_T^f is the final integrated state including all forcing terms, ψ_N^f is the final integrated state including only one of the three forcings, and ψ_0^f the final state from an unforced model integration. In general, this relationship does not have to be satisfied, as the inclusion of the different contributions to F_o alters ψ', which in turn modifies the evolution of the model fields. The difference between the rhs and lhs of (6) measures the degree to which each of the three forcing terms can be considered independently. We expect this difference to increase with the length of the integration. For a 3-day integration, for all lags and both cases, the magnitude of this term is typically less than 10% of that for either the lhs or rhs of (6) (not shown). This result also holds if (5) is limited to any combination of two of the three forcing terms.

Figures 8 through 10 show the anomaly from the barotropic model experiments targeted for the onset (lag 0), anomaly maximum (lag +5), and decay (lag +10) days, respectively, for the downstream case. Because the largest difference between the upstream and downstream cases is found during the decay phase, for the upstream case, we only show the case targeted for the decay day (Fig. 11). As stated earlier, the initial perturbation is the composite field 3 days before the target

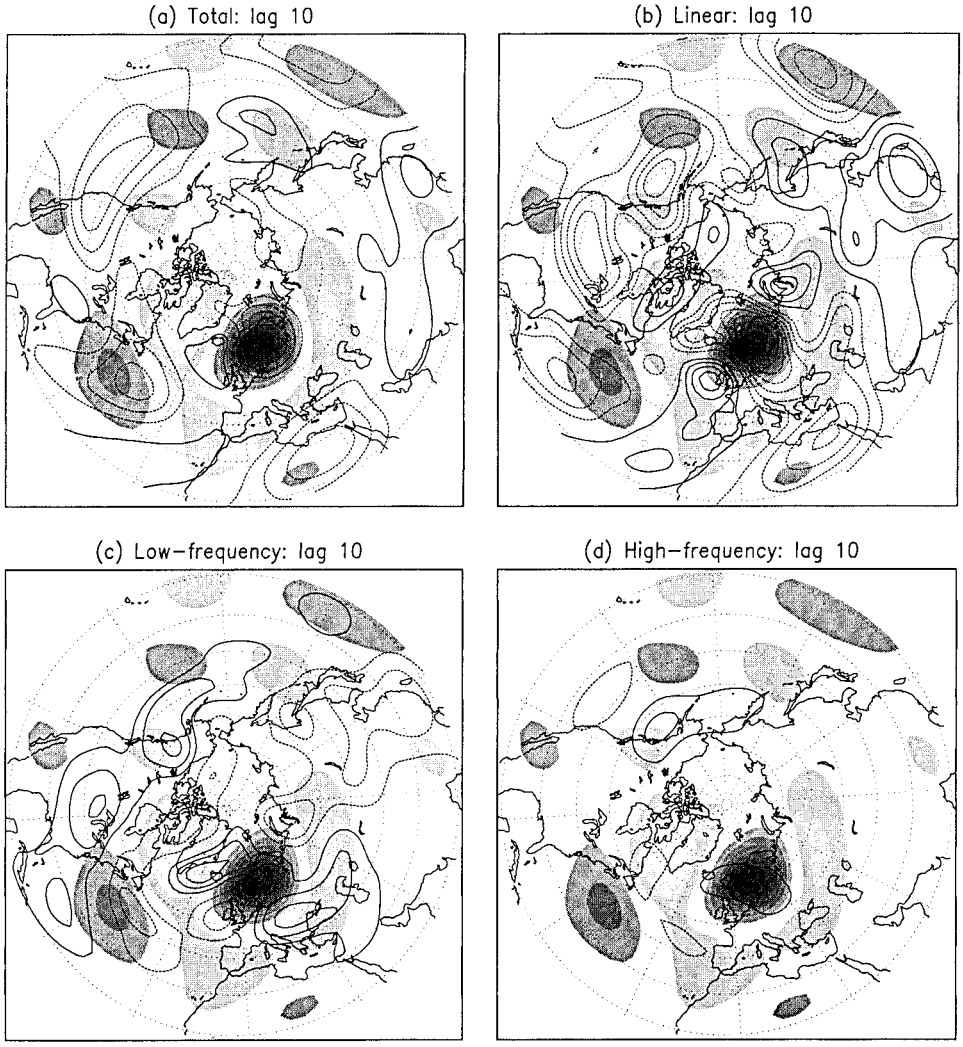

FIG. 7. As for Fig. 6, except that the budget terms are for lag +10.

day. The forced nonlinear integrations with F_o specified as the sum of all three forcing terms (this will be referred to as the fully forced model; see Figs. 8f, 9f, and 10f for the downstream case, Fig. 11f for the upstream case) reproduces the composite field (Figs. 2b–d for the downstream case, Fig. 3d for the upstream case) reasonably well. This result, together with the fact that (6) holds, enables us to dissect the impact of the individual forcing terms in (4). Therefore, we proceed to examine the following five sets of experiments: unforced linear, unforced nonlinear, forced nonlinear with F_o specified as the incoherent nonlinear term, the divergence term, and the high-frequency nonlinear term. Throughout the paper, the latter three experiments will be referred to collectively as ''partially forced model'' integrations.

a. Downstream case

We first examine the barotropic model experiments for the onset day. The unforced linear model (Fig. 8a) fails to produce key features of the fully forced model integration (Fig. 8f), such as the high west of Ireland, which subsequently evolves into the fully developed block. Furthermore, there is a negative anomaly over the Norwegian Sea, which is absent in Fig. 8f. The unforced nonlinear model (Fig. 8b) yields almost identical results to those produced by the linear model, suggesting that self-induced nonlinearity plays a minimal role. As will be shown below, for all calculations, the self-induced nonlinearity is found to be unimportant. Therefore, all results from the nonlinear model, when forced with the divergence term alone, can be regarded as representing the block evolution due solely to the linear terms. This point was verified by performing integrations of the linear model, forced with the divergence term alone (not shown).

Inclusion of the incoherent (Fig. 8c) and the high-frequency (Fig. 8e) nonlinear terms improves the accuracy only slightly. Each calculation introduces a weak high that partially overlaps with the block at the British

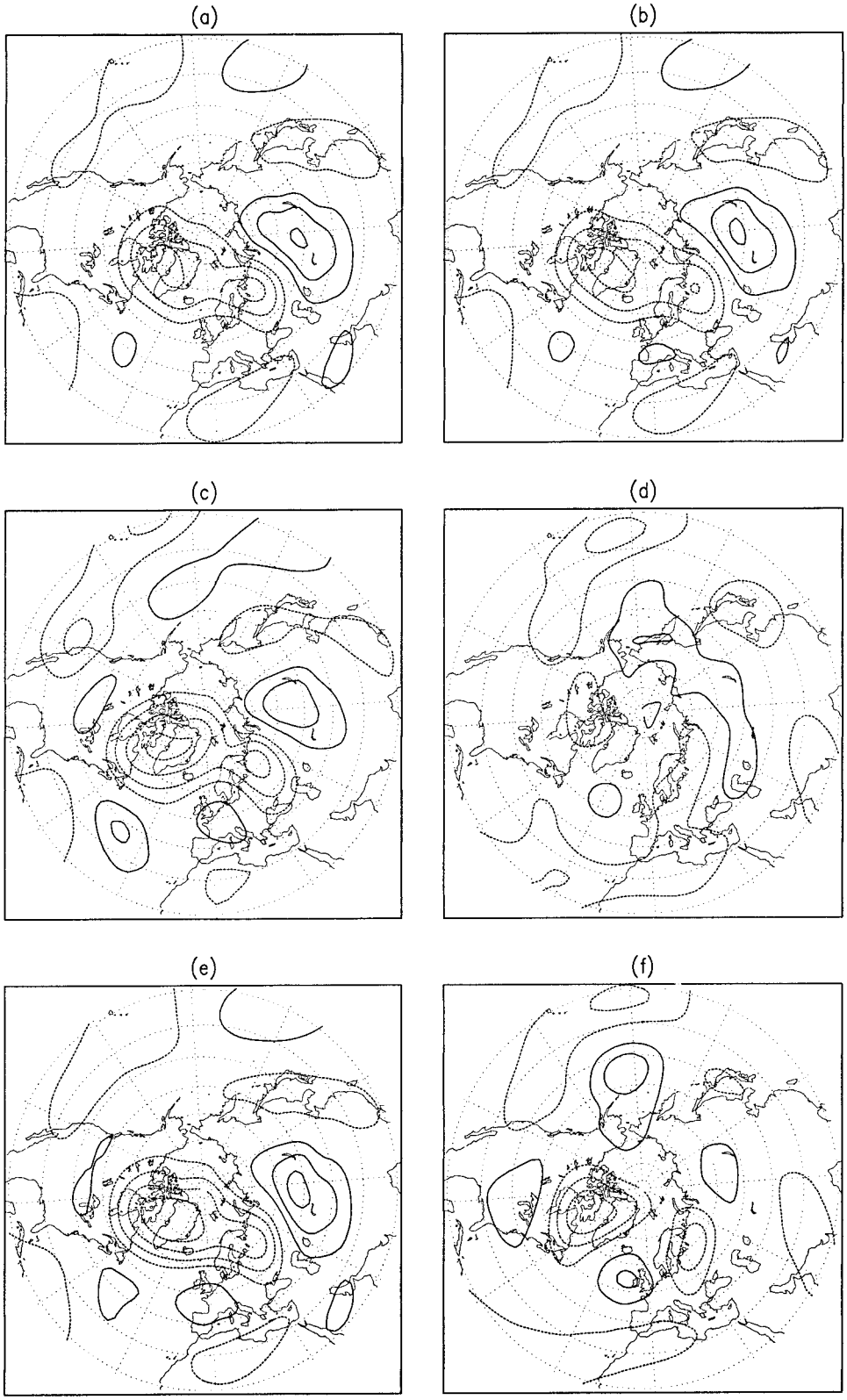

FIG. 8. The streamfunction anomaly from 3-day integration of the (a) linear barotropic model, nonlinear barotropic model with F_o in (4) being (b) zero, (c) the incoherent nonlinear term, (d) the divergence term, (e) the high-frequency nonlinear term, and (f) the sum of (c) through (e) for the downstream case. The models are initialized with the composite anomaly at lag −3. Solid (dashed) contours indicate positive (negative) values, and the contour interval is 2×10^6 m^2 s^{-1}. The zero contour is omitted.

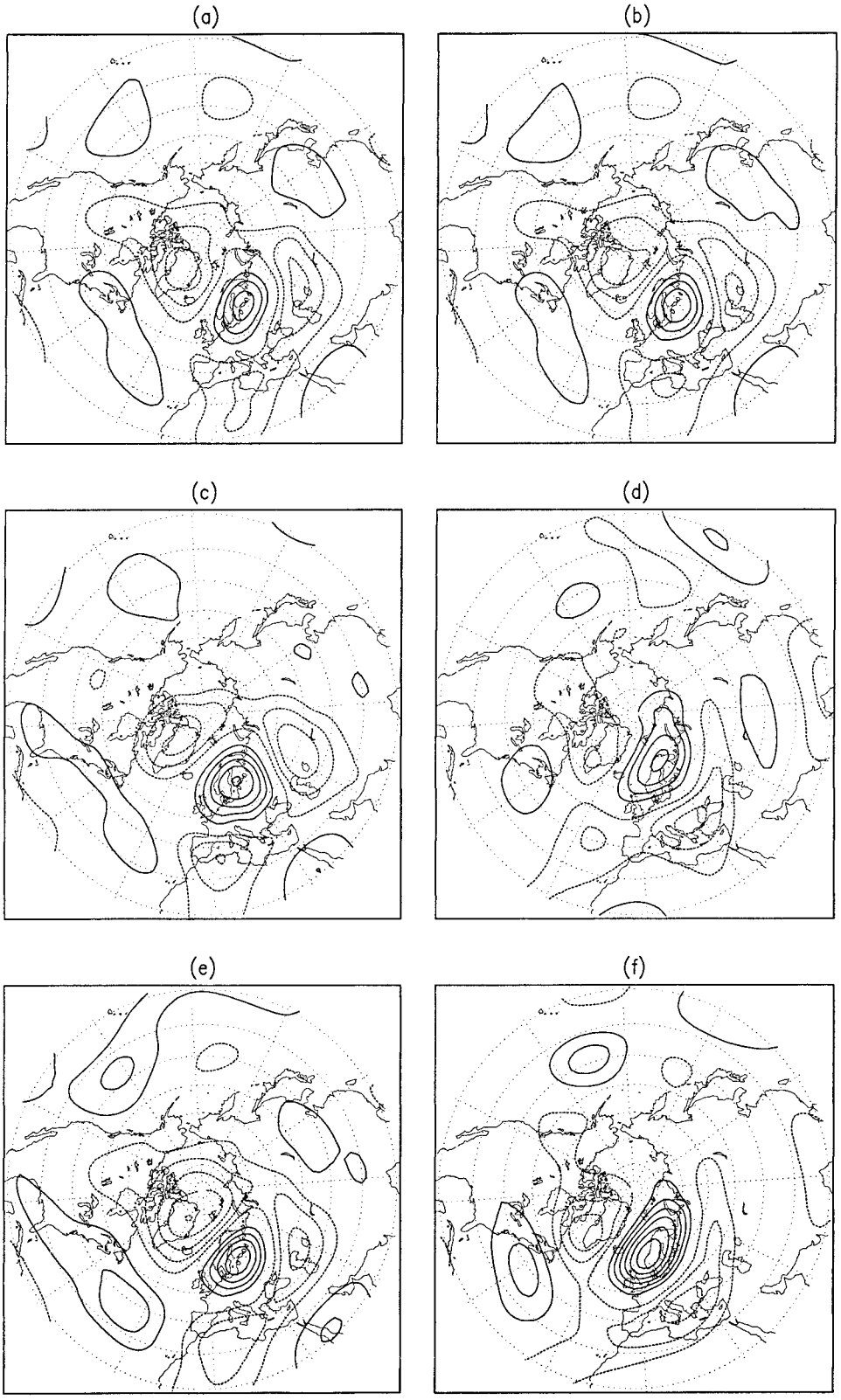

FIG. 9. As for Fig. 8, except that the models are initialized with the composite anomaly at lag +2.

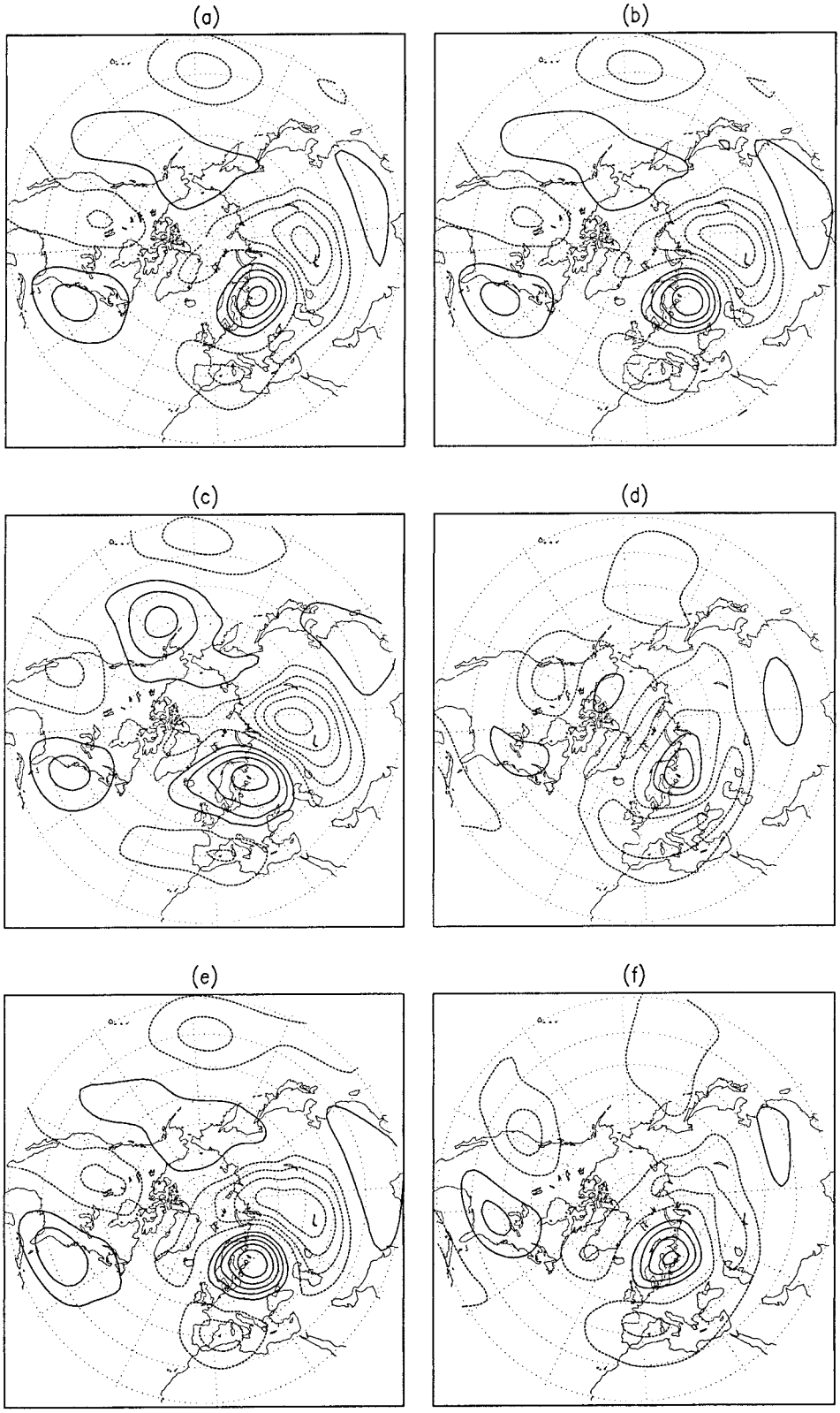

FIG. 10. As for Fig. 8, except that the models are initialized with the composite anomaly at lag +7.

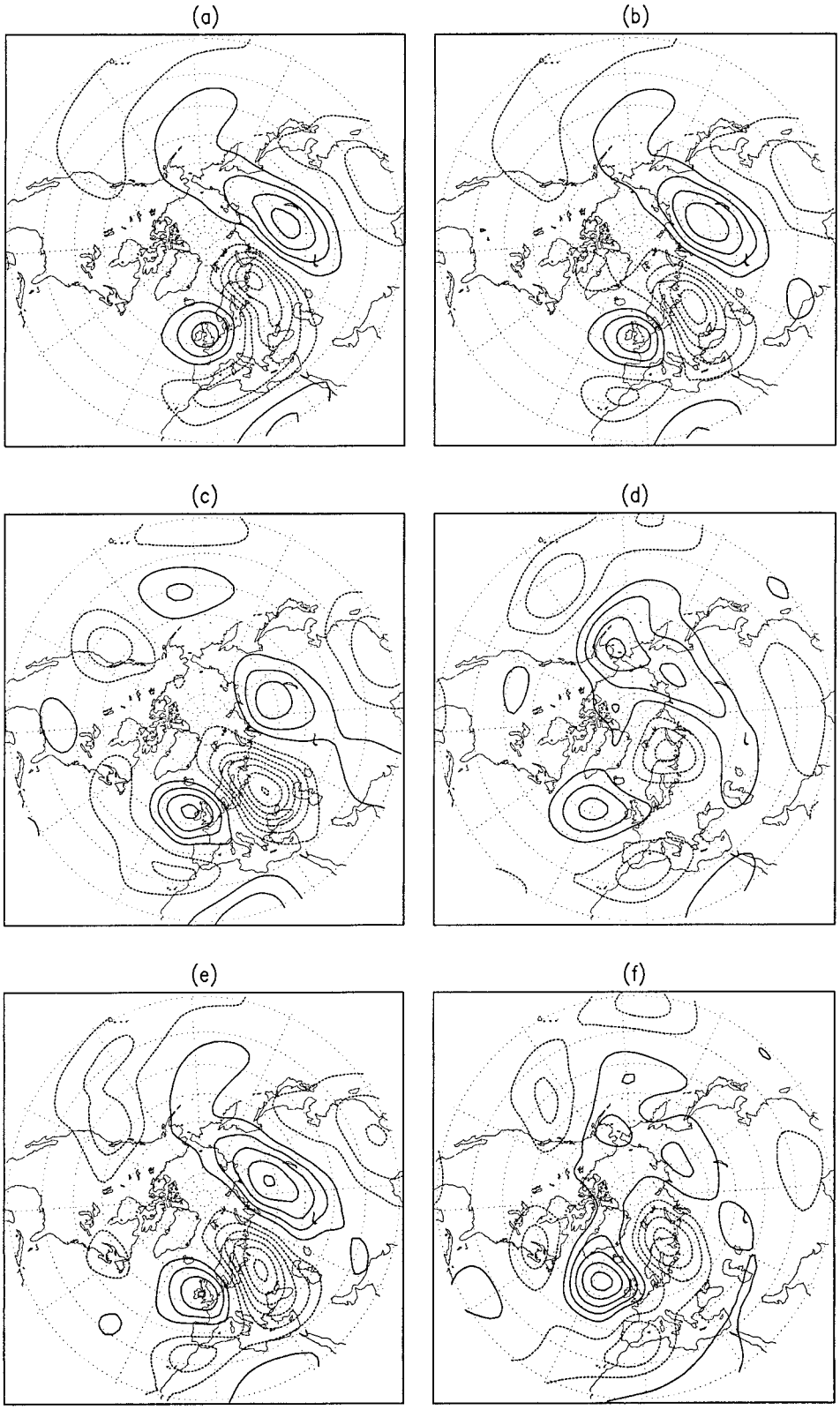

FIG. 11. As for Fig. 10, except for the upstream case.

Isles in Fig. 8f. Inclusion of the divergence term (Fig. 8d) produces significant changes, yielding a weak high 30° west of the British Isles, and greatly reducing the amplitude of the other anomalies. This results in an elimination of the negative anomaly north of the block and a lowering of the amplitude of the downstream positive anomaly. Comparing the results from the fully forced model calculation with those from each of the partially forced model runs, we conclude that all three of the forcing terms, including the divergence term, must be included in order to correctly produce the block.

Figures 9a and 9b show that both the linear and unforced nonlinear model cannot accurately capture the block maximum, producing anomalies that are too weak and propagate too rapidly downstream. The incoherent nonlinear term (Fig. 9c) now has a significant effect, increasing the block amplitude by nearly 50%. To a lesser degree, the high-frequency nonlinear term also amplifies the blocking high. Once again, the divergence term significantly alters the entire anomaly field; the negative anomaly centered over Kazakhstan in Figs. 9a–c and 9e shifts to the southwest. Interestingly, in this particular case, the divergence term also increases the amplitude of the blocking high. Both of the nonlinear terms (Figs. 9c,e) produce blocks located slightly west of the unforced counterpart (Fig. 9b), which is consistent with the location of the corresponding composite forcing terms shown in Figs. 7c and 7d. However, the blocks in Figs. 9c and 9e lie southeast of the block in the fully forced model (Fig. 9f), indicating that neither of the two nonlinear terms, by itself, is strong enough to drive the block sufficiently far upstream. As the divergence term drives the block northward (Fig. 9d) compared with the unforced and other partially forced model integrations, it is again found that all three of the forcing terms play a crucial role in determining the amplitude and structure of the block.

During the decay phase, the high-frequency nonlinear term amplifies the block (Fig. 10e); the incoherent nonlinear term expands the area of the block (Fig. 10c) while having little influence on its amplitude; and the divergence term causes the block to decay (Fig. 10d). Also, the divergence term plays a central role for the general structure of the anomalies, mainly by its influence on the negative anomalies surrounding the block. In contrast to the maintenance phase, the high-frequency nonlinear term plays more a important role in retaining the block amplitude than the incoherent nonlinear term. In summary, these results show that although all three forcing terms are involved in the evolution of the block, it is the divergence term that contributes the most to its decay.

b. Upstream case

Because key features of the upstream case are broadly similar to those of the downstream case, only a brief description is provided. As for the downstream case, inclusion of the self-induced nonlinearity has minimal effect, the incoherent nonlinear term is as important as the high-frequency nonlinear term in amplifying the block, and the divergence term substantially alters the evolution of the flow for all lags. By comparing Fig. 11d with all other panels in Fig. 11, it is clear that the divergence plays the most important role in retarding the downstream propagation of the blocking anomalies, and the amount of westward shifting by the divergence term is much greater than that for the downstream case (see Fig. 10).

5. Summary and discussion

This study examines the temporal evolution of blocking events over the Atlantic Ocean and Europe in a perpetual January GFDL GCM. Given that many of the previous studies on blocks emphasize the importance of storm track eddies, we investigate the evolution of blocks at two different locations: one close to the Atlantic storm track, and the other farther downstream. These are referred to as the upstream and downstream cases, respectively. The upstream case is associated with a wave train that propagates through the blocking region, while the downstream case is initiated by in situ development. To the extent that the dynamical processes of the blocks in a GCM are equivalent to those in the atmosphere, this result does not support the speculation of Nakamura et al. (1997), who suggested that blocks near the storm tracks form in situ while blocks farther removed from the storm track are more closely associated with wave trains.

The different formation characteristics, as described above, are manifested in the pattern covariance of each term in the streamfunction tendency equation with the maximum anomaly. Leading up to onset and shortly afterward, this calculation shows that the linear term dominates in the upstream case, while both the linear and the incoherent forcing terms dominate in the downstream case. However, as was shown in the barotropic model calculations, when the high-frequency nonlinear term is the sole forcing, the blocking high amplifies during the onset, although the location is incorrectly produced. This discrepancy between the covariance and the barotropic model results arises, in part, from the fact that the block is not a truly stationary feature. The discrepancy also shows that a complete picture requires the detailed analysis of the barotropic model experiment, even though the covariance calculation provides a useful guideline. The basic properties of the two cases are very similar at other times, with the linear term dominating the decay of the blocks, and the nonlinear terms prolonging the lifetime of the blocks by 2 to 3 days.

One factor that limits the interpretation of budget study results, such as those described above, is that, in general, the influence of each forcing term is not independent from the other. However, from a series of

barotropic model experiments, we show to a large degree that each of the three forcing terms, that is, the incoherent nonlinear, high-frequency nonlinear, and divergence terms, do behave independently for a period up to about 3 days. We then use this independence characteristic to investigate the role of the three forcing terms. For both cases, the barotropic model experiments find that the high-frequency and incoherent nonlinear terms are almost equally important for the maintenance of the block. On the other hand, the self-induced term is found to play a very minimal role. Because the incoherent nonlinear term is missing in the similar calculations performed by Nakamura et al. (1997), we suspect that the role of low-frequency nonlinearity is likely to be underestimated in their study. If that is the case, because they used observed data and blocking criteria different from ours, it is also unlikely that the large effect of the incoherent nonlinear term is simply due to our dataset and/or blocking criteria.

As stated earlier, because the incoherent nonlinear term arises from case-to-case variability of the low-frequency flow associated with individual blocking events, this term should be interpreted as being part of the self-induced nonlinear term. However, the large case-to-case variability of the low-frequency flow itself does not necessarily indicate that the composite block is completely misrepresentative of individual blocking events. This is because for a given blocking event, there is no reason to expect that the block itself accounts for the *entire* low-frequency flow. For example, it is not uncommon that a single blocking event is composed of several intrusions of low potential vorticity (PV) air into the blocking region [e.g., see Fig. 6 of Hoskins and Sardeshmukh (1987)]. This process would contribute toward both the high- and low-frequency components of the flow. Thus, we believe that the nonsteadiness of the blocks, as well as the case to case variability of individual blocks, account for the large-amplitude incoherent nonlinear term.

The barotropic model experiments also show that the divergence term must be included in order to correctly reproduce the location of the blocking high at all phases during its evolution. For that matter, the anomaly structure over the entire hemisphere is poorly represented if the divergence term is absent. Although both the high-frequency and incoherent nonlinear terms cause the block to retrograde, without the divergence term, the blocks still migrate downstream too quickly. This is particularly true for the upstream case. The importance of the divergence term was also noted by Mullen (1986), who indicated that the divergence term plays an important role in keeping the block stationary. However, its role for the longevity of the block is rather ambiguous, because the divergence term, in general, reduces the anomaly amplitude except during the mature phase of the downstream case. Such an ambiguity is not surprising, given that the secondary circulation driven by both Ekman pumping and vorticity fluxes can contribute toward the divergence term.

The above results indicate that the low-frequency nonlinearity is as important as the high-frequency nonlinearity in prolonging the lifetime of the block. This contrasts the findings of previous studies that suggest that driving by high-frequency nonlinearities is the dominant forcing mechanism for both the initiation and maintenance of blocks (e.g., Shutts 1983; Mullen 1987; Nakamura and Wallace 1993). Such an inconsistency can, in part, be explained by the fact that all budget studies of blocks (e.g., Illari 1984; Mullen 1986, 1987) examine time-averaged properties, rather than the entire time evolution. In order to compare our results with previous diagnostic studies, we perform a time average of each of the budget terms. For this calculation, to be consistent with previous studies, the composites are obtained relative to the time of the blocking anomaly maximum.[2]

Figure 12 shows the time-averaged budget terms for the downstream case. As expected, compared with the individual budget terms, the time mean of the sum of the budget terms (Fig. 12a) is small. The linear terms (Fig. 12b) advect the block downstream, although the positive tendency in the downstream half of the block is rather weak. This tendency is canceled mainly by the high-frequency nonlinear term (Fig. 12d). This is consistent with Mullen (1986, 1987), although the former did not separate the nonlinear term into high- and low-frequency components, and the latter examined the potential vorticity, rather than the vorticity, budget. Compared with the high-frequency nonlinear term, the low-frequency nonlinear term appears to play a much lesser role in maintaining the block, as there are regions where negative values of the low-frequency nonlinear term overlap with the blocking high, and the positive values are found in the southeastern as well as northwestern part of the block (Fig. 12c). However, as we have seen in the barotropic model experiments, the low-frequency nonlinear term is as important as the high-frequency nonlinear term for maintaining the block. Evidently, the high-frequency nonlinearity dominates the time-averaged budget because the sign and structure of that term, compared with those of the low-frequency nonlinear term, change very little over the lifetime of the block. Thus, time-averaged budget maps can be misleading by failing to capture important details, such as the role of linear terms for the onset and the relative importance of the low-frequency nonlinear term.

The results of the barotropic model experiments also allow us to address the relevance of nearly stationary

[2] When the composites are performed relative to the time of the blocking maximum, it is found that the temporal evolution of the composite budget terms and anomalies (not shown) strongly resemble their counterparts presented in section 3, indicating that the results in this study are robust against the choice of base day.

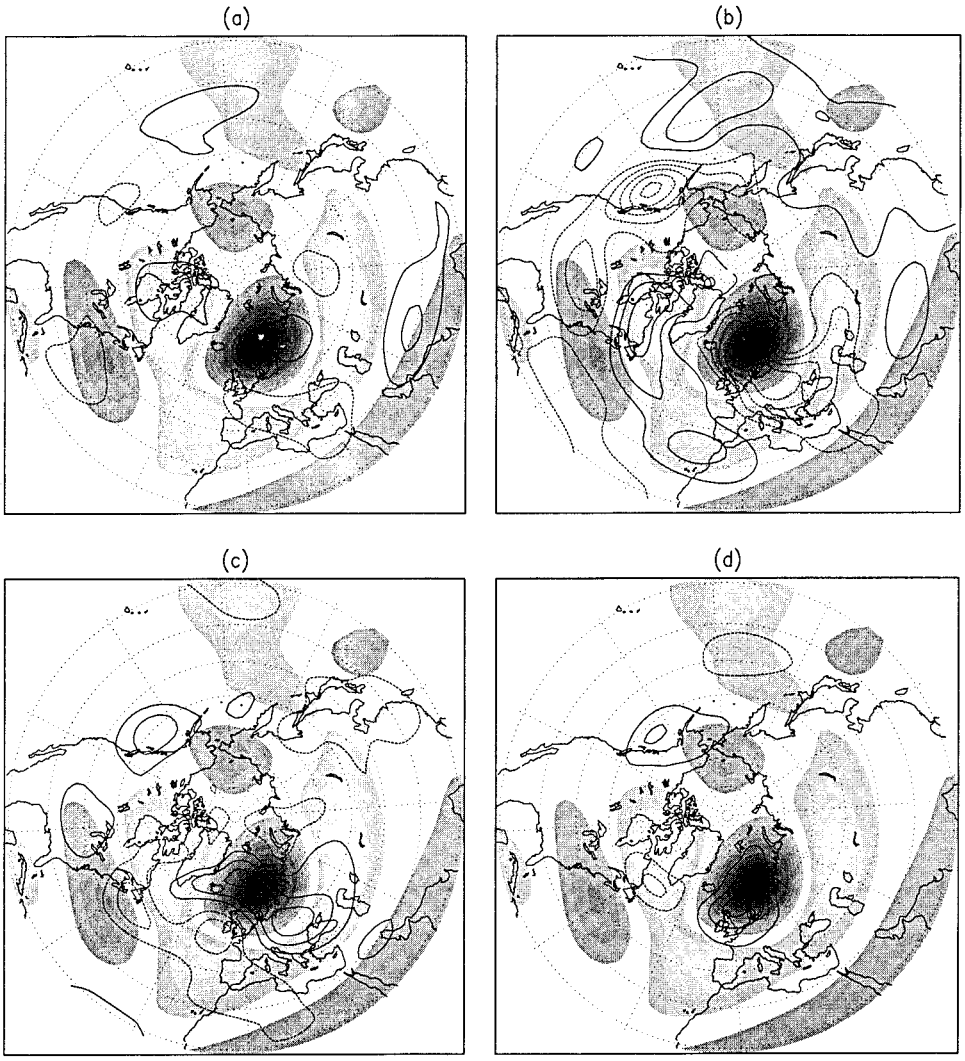

FIG. 12. As for Fig. 5, except that the budget terms are averaged over a period from lag −6 to lag +6, and the composites are obtained relative to the blocking anomaly maximum. Shading indicates composite streamfunction anomaly averaged over the same time period, with contour interval 1×10^6 m^2 s^{-1}.

states (NSSs) for the maintenance of blocks. For the sake of clarity, consider the nondivergent, inviscid, unforced barotropic vorticity equation:

$$\frac{\partial}{\partial t}\nabla^2\psi_s = -J(\psi_s, \nabla^2\psi_s + f) \approx 0, \qquad (7)$$

where the subscript s represents an NSS and the remaining notations are standard. Given an observed flow that contains a block, by minimizing the rhs of (7), Anderson (1992) obtained an NSS that retains a feature resembling a modon (Butchart et al. 1989). If we are to make an analogy between our composite block and the NSS, a zero tendency in (7) amounts to a balance between our linear terms, excluding the divergence term, and the self-induced nonlinear term. Therefore, the importance of the self-induced nonlinearity measures the degree to which the NSS paradigm is valid for the composite block. Because the role of the self-induced nonlinear term is shown to be minimal, we conclude that an NSS is of very little relevance for the *composite* block in our study. However, as stated earlier, it should be noted that the same conclusion cannot be drawn for any individual block that comprises the composite. This is because the structure of an individual block does not have to be exactly the same as that of the composite block. Thus, for those NSSs that correspond to individual blocks, because of case to case variability between NSSs, it is possible that *part* of the incoherent nonlinear term contributes toward the rhs of (7). Provided that the entire high-frequency nonlinear term represents the eddy straining mechanism, because the high- and low-frequency nonlinear terms are equally important, and because not all low-frequency nonlinear terms can be attributed to the NSS, we conclude that,

in general, the eddy straining mechanism is more relevant than the NSS for the block maintenance.

Our results also offer an explanation for the fact that the blocks in NSSs are always stronger than their counterparts in the atmosphere (Anderson 1992). After separating the rhs of (7) into linear and nonlinear terms, the stationarity of the block is achieved when the nonlinear term that drives the block upstream balances the linear term that advects the block downstream. As we have shown, the divergence term can be crucial in retarding the downstream propagation of the block. Therefore, a balance between linear and nonlinear terms that neglects divergence requires a stronger nonlinear term, hence stronger anomalies.

Acknowledgments. This research was supported by the National Science Foundation through Grants ATM-9416701 and ATM-9712824. Comments by Dr. Feldstein on an early version of the manuscript are greatly appreciated. Thanks are also due to two anonymous reviewers whose comments helped to improve the manuscript.

REFERENCES

Anderson, J. L., 1992: Barotropic stationary states and persistent anomalies in the atmosphere. *J. Atmos. Sci.,* **49,** 1709–1722.

Berggren, R., B. Bolin, and C.-G. Rossby, 1949: An aerological study of zonal motion, its perturbations and break-down. *Tellus,* **1,** 14–37.

Blackmon, M. L., S. L. Mullen, and G. T. Bates, 1986: The climatology of blocking events in a perpetual January simulation of a spectral general circulation model. *J. Atmos. Sci.,* **43,** 1379–1405.

Branstator, G., 1992: The maintenance of low-frequency atmospheric anomalies. *J. Atmos. Sci.,* **49,** 1924–1945.

——, and J. D. Opsteegh, 1989: Free solutions of the barotropic vorticity equation. *J. Atmos. Sci.,* **46,** 1799–1814.

Butchart, N., K. Haines, and J. C. Marshall, 1989: A theoretical study of solitary waves and atmospheric blocking. *J. Atmos. Sci.,* **46,** 2063–2078.

Cai, M., and H. M. Van den Dool, 1994: Dynamical decomposition of low-frequency tendencies. *J. Atmos. Sci.,* **51,** 2086–2100.

Colucci, S. J., 1985: Explosive cyclogenesis and large-scale circulation changes: Implications for atmospheric blocking. *J. Atmos. Sci.,* **42,** 2701–2717.

Dole, R. M., and N. D. Gordon, 1983: Persistent anomalies of the extratropical Northern Hemisphere wintertime circulation: Geographical distribution and regional persistence characteristics. *Mon. Wea. Rev.,* **111,** 1567–1586.

Feldstein, S., 1998: The growth and decay of low-frequency anomalies in a GCM. *J. Atmos. Sci.,* **55,** 415–428.

Fredrickson, J. S., 1982: A unified three-dimensional instability theory of the onset of blocking and cyclogenesis. *J. Atmos. Sci.,* **39,** 969–982.

Gordon, C. T., and W. F. Stern, 1982: A description of the GFDL spectral model. *Mon. Wea. Rev.,* **110,** 625–644.

Hoskins, B. J., and P. D. Sardeshmukh, 1987: A diagnostic study of the dynamics of the Northern Hemisphere winter of 1985–86. *Quart. J. Roy. Meteor. Soc.,* **113,** 759–778.

Illari, L., 1984: A diagnostic study of the potential vorticity in a warm blocking anticyclone. *J. Atmos. Sci.,* **41,** 3518–3526.

Kaas, E., and G. Branstator, 1993: The relationship between a zonal index and blocking activity. *J. Atmos. Sci.,* **50,** 3061–3077.

Liu, Q., 1994: On the definition and persistence of blocking. *Tellus,* **46A,** 286–297.

Mak, M., 1991: Dynamics of an atmospheric blocking as deduced from its local energetics. *Quart. J. Roy. Meteor. Soc.,* **117,** 477–493.

McWilliams, J. C., 1980: An application of equivalent modons to atmospheric blockings. *Dyn. Atmos. Oceans,* **5,** 43–46.

Mullen, S. L., 1986: The local balances of vorticity and heat for blocking anticyclones in a spectral general circulation model. *J. Atmos. Sci.,* **43,** 1406–1441.

——, 1987: Transient eddy forcing of blocking flows. *J. Atmos. Sci.,* **44,** 3–22.

Nakamura, H., and J. M. Wallace, 1993: Synoptic behavior of baroclinic eddies during the blocking onset. *Mon. Wea. Rev.,* **121,** 1892–1903.

——, M. Nakamura, and J. L. Anderson, 1997: The role of high- and low-frequency dynamics in blocking formation. *Mon. Wea. Rev.,* **125,** 2074–2093.

Shutts, G. J., 1983: The propagation of eddies in diffluent jetstreams: Eddy vorticity forcing of ''blocking'' flow fields. *Quart. J. Roy. Meteor. Soc.,* **109,** 737–761.